SIAM J. APPL. ALGEBRA GEOMETRY
Vol. 1, pp. 459–483

A Flexible C^2 Subdivision Scheme on the Sphere: With Application to Biomembrane Modelling*

Jingmin Chen†, Sara Grundel‡, and Thomas P. Y. Yu§

Abstract. We construct a C^2 multiscale approximation scheme for functions defined on the (Riemann) sphere. Based on a three-directional box-spline, a flexible C^2 scheme over a valence 3 extraordinary vertex can be constructed. Such a flexible C^2 subdivision scheme is known to be impossible for arbitrary valences. The subdivision scheme can be used to model spherical surfaces based on a recursively subdivided tetrahedron, with only valence 3 and 6 vertices in the resulted triangulations. This adds to the toolbox of subdivision methods a high order, high regularity scheme which can be beneficial to scientific computing applications. For instance, the scheme can be used in the numerical solution of the Canham–Helfrich–Evans models for spherical and toroidal biomembranes. Moreover, the characteristic maps of the subdivision scheme endow the underlying simplicial complex with a conformal structure. This in particular means that the special subdivision surfaces constructed here comes with a well-defined harmonic energy functional, which can in turn be exploited to promote conformality in surface parameterizations. We develop an efficient parallel algorithm for computing the harmonic energy and its gradient with respect to the control vertices. A software implementation (in CUDA and MATLAB) is provided.

Key words. subdivision schemes, sphere, biomembranes, curvature

AMS subject classifications. 65D07, 65D15, 65D17, 65D10, 65Z05, 65Y05

DOI. 10.1137/16M1076794

1. Introduction.

Subdivision surfaces are a standard technique for modeling free-form surfaces in computer animation. A major technical breakthrough in its development is the ability to extend box-splines to handle surfaces of an arbitrary topology. At a finer level the arbitrary topology problem amounts to dealing with "extraordinary vertices." Since Euler characteristics tell us that these extraordinary vertices cannot be avoided in the arbitrary topology setting, the ability to construct well-behaved extraordinary vertex subdivision rules is the key to making subdivision surfaces applicable to the free-form setting. A mathematical theory for analyzing these extraordinary vertex rules has therefore been developed; see, for example, [21, 24, 29, 32, 31] and the references therein.

The construction of flexible curvature continuous subdivision schemes over extraordinary vertices is a well-known difficult problem. It is known from a result of Prautzsch and Reif

*Received by the editors May 24, 2016; accepted for publication (in revised form) March 2, 2017; published electronically August 17, 2017.
http://www.siam.org/journals/siaga/1/M107679.html
Funding: The second author was supported in part by National Science Foundation grant DMS 0714321. The third author was supported in part by National Science Foundation grants DMS 0512673 and DMS 0915068.
†Citigroup Global Markets, New York, NY 10013 (jingmchen@gmail.com).
‡Max Planck Institute for Dynamics of Complex Technical Systems, 39106 Magdeburg, Germany (grundel@mpi-magdeburg.mpg.de).
§Department of Mathematics, Drexel University, Philadelphia, PA 19104 (yut@drexel.edu).

[23] that it is impossible to construct a flexible C^2 scheme over extraordinary vertices unless the regular subdivision scheme (assumed in [23] to be based on polynomial splines) is capable of producing polynomial patches of total degree 8 in the triangle case and bidegree 6 in the quadrilateral case. Prautzsch and Reif's degree estimate, however, comes with a caveat, namely, that in the triangle mesh setting it is not applicable to the valence 3 case. In fact, the result in [23] is inconclusive about this valence 3 case.

Using a method called jet subdivision, it was shown that a C^2 scheme with the same subdivision stencils as the Loop scheme [17] actually exists in the valence 3 case, but the scheme requires the use of order 1 jet data and also it does not generate polynomial patches [30] for general control data. We show in this paper that it is possible to obtain a similar C^2 construction without using jets. Moreover, the scheme developed in this paper, which we call the "C2g0 scheme," is based on a relatively simple three-directional box-spline, instead of a noninterpolatory Hermite subdivision scheme [13], which does not generate piecewise polynomials.

Our proof (section 2) demystifies the flexible C^2 scheme constructed in [30] and also explains why Prautzsch and Reif's degree estimate does not hold in the valence 3 case.[1]

1.1. Applied motivations. Besides filling in a theoretical gap, another motivation for constructing such a smooth valence 3 scheme comes from the general interest in approximating spherical (i.e., genus 0) surfaces or functions defined on a spherical domain [26, 19, 10, 18, 12]. Note that a multiscale triangulation of a spherical domain can be constructed based on recursively subdividing a tetrahedron; such triangulations of the sphere consist only of valence 3 and 6 vertices. The subdivision scheme developed here thus gives rise to a smooth multiresolution analysis (MRA) on the topological sphere.

The authors' primary applied interest is the numerical solution of the Canham–Helfrich–Evans models [2, 14, 8, 27] for biomembranes. In one version of the models, one seeks a surface of a prescribed genus g that solves the following variational problem:

$$\min_S \overbrace{\int_S H^2\,dA}^{=:\text{Willmore}(S)} \quad \text{s.t.} \quad \begin{cases} \text{(i)} & \text{area}(S) = \int_S 1\,dA = A_0, \\ \text{(ii)} & \text{volume}(S) = \frac{1}{3}\int_S [x\hat{\mathbf{i}} + y\hat{\mathbf{j}} + z\hat{\mathbf{k}}]\cdot\hat{\mathbf{n}}\,dA = V_0, \\ \text{(iii)} & \text{total-mean-curvature}(S) := \int_S H\,dA = M_0. \end{cases} \tag{1.1}$$

In the above, the constraint values (A_0, V_0, M_0) are fixed (typically by the temperature of the environment and the type of phospholipid); the minimum is taken over all regular enough genus g surfaces S.

In [5, 4], we develop a parallel and high accuracy order numerical method for solving the problem based on subdivision methods. The development there is mainly based on the Loop subdivision scheme, but the cases of $g = 0, 1$ can also be implemented based on the C2g0 scheme. Compared to Loop, the C2g0 scheme

(i) has a higher regularity (C^1 for Loop versus C^2 for C2g0) at extraordinary (valence 3) vertices, and

[1] We thank H. Prautzsch for clarifying a key argument in [23]. After the completion of our original manuscript [11] in 2011, we learned that the same idea was carried out by Karciauskas and Peters [16] in the quadrilateral case. Their study was motivated by an application rather different from those discussed in section 1.1.

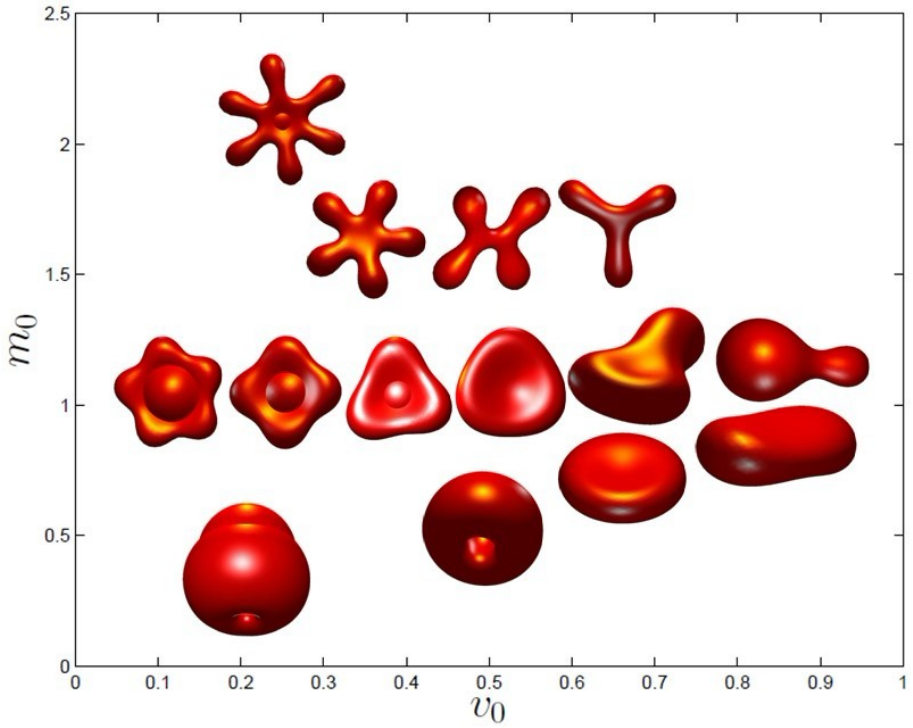

Figure 1. *Approximate solutions of (1.1) for various (A_0, V_0, M_0) using the C2g0 subdivision scheme constructed in this paper, reproduced from Chen's Ph.D. thesis [4]. Due to a scale invariance of the problem, the solution surface depends, up to homotheties, only on the so-called reduced volume $v_0 := V_0/[(4\pi/3)(A_0/4\pi)^{3/2}]$ and the reduced total mean curvature $m_0 := M_0/[4\pi(A_0/4\pi)^{1/2}]$.*

(ii) has a higher approximation order (order 4 for Loop versus order 6 for C2g0) in the regular setting.

Since the spherical topology (i.e., $g = 0$) is arguably the most important topology in cell biology, it is helpful to have such a method with higher approximation order and regularity. See, for instance, Figure 7. For this particular application, the superior performance of C2g0 is likely attributable more to (ii) than to (i). Yet, the C^2 regularity enjoyed by C2g0 makes the computation of the Willmore energy slightly more efficient: unlike a Loop surface, curvature of C2g0 surface does not blow up, and is continuous, in the vicinity of any valence 3 vertex.[2]

The genus 0 surfaces in Figure 1 are obtained by solving (1.1) using the C2g0 subdivision scheme.

1.2. Three directional box splines. Recall that a standard subdivision surface scheme is constructed based on a subdivision scheme in the regular grid setting followed by construction of special extraordinary vertex rules. In this section, we discuss the specific regular subdivision scheme used in the construction in this paper. In section 2, we show how a flexible C^2 scheme can be constructed in the valence 3 case.

[2]Details of numerical integration are discussed in [5, 4].

The standard Loop scheme is based on the three directional box spline with directions $[1,0]$, $[0,1]$, $[1,1]$ each repeated twice. Recall the following definition of box-spline [22, 6]: Let $\Xi = \{v_1, v_2, \ldots, v_k\}$ be a set of k vectors in $\mathbb{R}^2$ with the first two vectors being linearly independent. The box-spline function B_Ξ is defined as follows. Let B_2 be the indicator function on the parallelogram $[v_1, v_2][0,1)^2$, scaled by the constant $1/\det[v_1, v_2]$, i.e., $B_2 := 1_{[v_1,v_2][0,1)^2}/\det[v_1, v_2]$. Then define $B_3, \ldots, B_k =: B_\Xi$ recursively by

$$B_\kappa(x) = \int_0^1 B_{\kappa-1}(x - tv_\kappa)\, dt, \quad \kappa > 2. \tag{1.2}$$

When the direction vectors have integral entries, the box spline $B_\Xi(x)$ can be generated by a dyadic subdivision scheme, which also means that it satisfies a refinement equation of the form $B_\Xi(x) = \sum_{\alpha\in\mathbb{Z}^2} a_\alpha B_\Xi(2x - \alpha)$.

In this paper we consider the three directional box spline with directions $[1,0]$, $[0,1]$, $[1,1]$ each repeated thrice. This box spline can be generated by a subdivision scheme whose mask $(a_\alpha)_\alpha$ has the following symbol (z-transform):

$$\sum_{\alpha\in\mathbb{Z}^2} a_\alpha z_1^{\alpha_1} z_2^{\alpha_2} =: \widehat{a}(z_1, z_2) = z_1^{-3} z_2^{-3}(1 + z_1)^3(1 + z_2)^3(1 + z_1 z_2)^3/128. \tag{1.3}$$

(For the connections among box-splines, subdivision schemes, and refinement equations, consult [3, 6, 22].)

Since this scheme has the usual hexagonal symmetry of the regular triangular grid, it can be used to construct subdivision surfaces in the arbitrary topology setting; the vertex and edge rules associated with the mask (1.3) are shown in Figure 2. Notice that the vertex rule has the same stencil as that of the Loop scheme; the edge rule, however, has a bigger stencil compared to Loop's but is still dependent only on the data in the 1-rings of the two end vertices of the edge.

Using standard sum rule conditions from subdivision theory, one can show that this subdivision scheme is the one and only one, among all the schemes with the same support, that reproduces all polynomials of total degree 4. In fact, this scheme also reproduces polynomials of total degree 5. On the other hand, the box-spline function associated with (1.3) consists of degree 7 polynomial pieces (easy to see from (1.2), as each integration increases the degree by 1), and it is C^4 smooth.

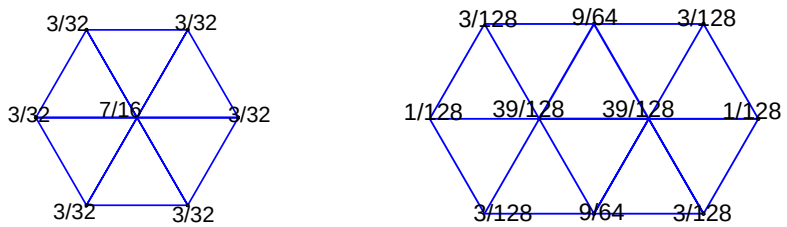

(a) vertex rule (b) edge rule, with a marquise-shaped stencil

Figure 2. *Subdivision rules for the box spline with directions* $[1,0]$,$[0,1]$,$[1,1]$ *each repeated thrice.*

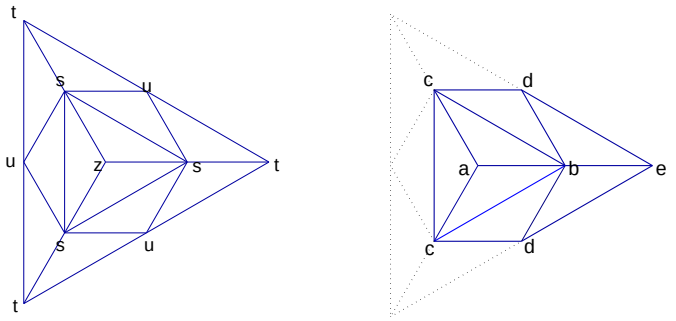

(a) extraordinary vertex rule $z = 1 - 3(s + t + u)$ (b) extraordinary edge rule $a = 1 - b - 2(c + d) - e$

Figure 3. *Valence* 3 *extraordinary vertex rules. By the end of section* 2*, the weights will be chosen to be* $(z, s, t, u) = (8901,\ 12606,\ 885,\ 2806)/57792$ *and* $(a, b, c, d, e) = (233,\ 248,\ 171,\ 29,\ 15)/896$*. The overall subdivision scheme will be called the C2g0 scheme.*

2. Valence 3 extraordinary vertex rules.

In this section, we develop a valence 3 extraordinary vertex rule based on the regular rules in Figure 2. For this purpose, it suffices to work on the 3-regular complex; see Figure 4. Recall that the 3-regular complex has a central valence 3 extraordinary vertex with all other vertices being ordinary (valence 6). Away from the extraordinary vertex, our subdivision scheme uses the rules in Figure 2. In the vicinity of the valence 3 vertex, our proposed subdivision rules have the stencils, together with the weights labeled and to be determined, specified in Figure 3. The goal of this section is to determine a set of weights that give rise to a flexible C^2 scheme. Note that, according to Prautzsch and Reif's degree estimate [23], such a C^2 scheme is impossible for any valence greater than 3 other than 6.

We begin with some well-known ideas in subdivision surface theory and gradually move toward the less well-known observations.

2.1. Linear algebra.

Like any other standard subdivision scheme, our scheme is *stationary*, meaning that the same set of rules is used at *all* levels. Together with the fact that these subdivision rules are linear, it is hardly surprising that eigendecomposition plays a key role in the analysis of subdivision schemes.

Given the support size of our proposed scheme, we need to use three rings of data around the extraordinary vertex in order to determine the subdivision limit function on the 1-disc (colored region in Figure 4(a)) around the extraordinary vertex. On the other hand, it is enough to use just two rings of data around the extraordinary vertex in order to determine the value of the limit function at the extraordinary vertex. Thus, the *subdivision matrix* of our scheme has the following block form:

$$S = \begin{bmatrix} M & 0 \\ A & B \end{bmatrix} \tag{2.1}$$

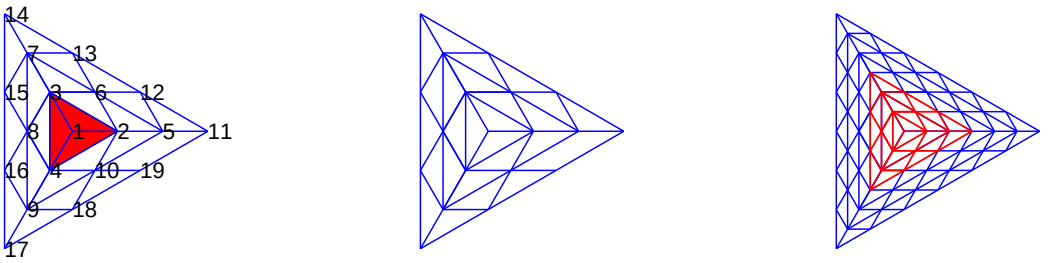

(a) ordering of vertices; in red: the 1-disc around the e.v. (denoted by D)

(b) level 0 complex

(c) level 1 (once subdivided) complex

Figure 4. *Ordering and subdivision of the* 3*-regular complex.*

if we order the vertices in the 3-regular complex as shown in Figure 4(a). Here,

$$M = \begin{pmatrix} z & s & s & s & t & u & t & u & t & u \\ a & b & c & c & e & d & 0 & 0 & 0 & d \\ a & c & b & c & 0 & d & e & d & 0 & 0 \\ a & c & c & b & 0 & 0 & 0 & d & e & d \\ 3/32 & 7/16 & 3/32 & 3/32 & 3/32 & 3/32 & 0 & 0 & 0 & 3/32 \\ 9/64 & 39/128 & 39/128 & 3/64 & 3/128 & 9/64 & 3/128 & 1/128 & 0 & 1/128 \\ 3/32 & 3/32 & 7/16 & 3/32 & 0 & 3/32 & 3/32 & 3/32 & 0 & 0 \\ 9/64 & 3/64 & 39/128 & 39/128 & 0 & 1/128 & 3/128 & 9/64 & 3/128 & 1/128 \\ 3/32 & 3/32 & 3/32 & 7/16 & 0 & 0 & 0 & 3/32 & 3/32 & 3/32 \\ 9/64 & 39/128 & 3/64 & 39/128 & 3/128 & 1/128 & 0 & 1/128 & 3/128 & 9/64 \end{pmatrix} \tag{2.2}$$

is the 10×10 matrix that maps the 2-ring data from one scale to the 2-ring data in the next finer scale, whereas the whole 19×19 matrix S maps the 3-ring data from one scale to the 3-ring data in the next scale. The entries in the blocks A and B come solely from the regular rules in Figure 2:

$$A = \frac{1}{128}\begin{pmatrix} 1 & 39 & 3 & 3 & 39 & 18 & 0 & 0 & 0 & 18 \\ 3 & 39 & 18 & 1 & 18 & 39 & 3 & 0 & 0 & 3 \\ 3 & 18 & 39 & 1 & 3 & 39 & 18 & 3 & 0 & 0 \\ 1 & 3 & 39 & 3 & 0 & 18 & 39 & 18 & 0 & 0 \\ 3 & 1 & 39 & 18 & 0 & 3 & 18 & 39 & 3 & 0 \\ 3 & 1 & 18 & 39 & 0 & 0 & 3 & 39 & 18 & 3 \\ 1 & 3 & 3 & 39 & 0 & 0 & 0 & 18 & 39 & 18 \\ 3 & 18 & 1 & 39 & 3 & 0 & 0 & 3 & 18 & 39 \\ 3 & 39 & 1 & 18 & 18 & 3 & 0 & 0 & 3 & 39 \end{pmatrix}, \quad B = \frac{1}{128}\begin{pmatrix} 1 & 3 & 0 & 0 & 0 & 0 & 0 & 0 & 3 \\ 0 & 3 & 1 & 0 & 0 & 0 & 0 & 0 & 0 \\ 0 & 1 & 3 & 0 & 0 & 0 & 0 & 0 & 0 \\ 0 & 0 & 3 & 1 & 3 & 0 & 0 & 0 & 0 \\ 0 & 0 & 0 & 0 & 3 & 1 & 0 & 0 & 0 \\ 0 & 0 & 0 & 0 & 1 & 3 & 0 & 0 & 0 \\ 0 & 0 & 0 & 0 & 0 & 3 & 1 & 3 & 0 \\ 0 & 0 & 0 & 0 & 0 & 0 & 0 & 3 & 1 \\ 0 & 0 & 0 & 0 & 0 & 0 & 0 & 1 & 3 \end{pmatrix}. \tag{2.3}$$

The spectrum of S is the union of the spectra of M and B. The eigenvalues of the 9×9 matrix B are $1/32$, $1/64$, $1/128$, each repeated thrice. As we will see, the six dominant eigenvalues of S will be constructed to be $1, 1/4, 1/4, 1/16, 1/16, 1/16$, so these eigenvalues must come from the spectrum of M.

The rotational and reflectional symmetries of a subdivision scheme are necessary for applying it to the arbitrary topology setting. Rotational symmetry, alone, implies a block circulant structure in the subdivision matrix S and also the submatrix M. This, in turn, implies that M can be block-diagonalized by a suitable Fourier matrix.

One may not immediately see the block circulant structure in (2.2), but that is just an artifact of the way we order the vertices: the ordering in Figure 3(a) is designed to give us the block structure in (2.1). To see the block circulant structure in M, simply reorder the

vertices in the first two rings according to the following permutation:

$$\begin{pmatrix} 1 & 2 & 3 & 4 & 5 & 6 & 7 & 8 & 9 & 10 \\ 1 & 2 & 5 & 8 & 3 & 4 & 6 & 7 & 9 & 10 \end{pmatrix}. \tag{2.4}$$

If P is the corresponding row permutation matrix, then

$$\widetilde{M} := PMP^T = \begin{bmatrix} z & \mathbf{v}^T & \mathbf{v}^T & \mathbf{v}^T \\ \mathbf{w} & \mathbf{C}_0 & \mathbf{C}_1 & \mathbf{C}_2 \\ \mathbf{w} & \mathbf{C}_2 & \mathbf{C}_0 & \mathbf{C}_1 \\ \mathbf{w} & \mathbf{C}_1 & \mathbf{C}_2 & \mathbf{C}_0 \end{bmatrix}, \tag{2.5}$$

where $\mathbf{v} = [s \;\; t \;\; u]^T$, $\mathbf{w} = [a \;\; 3/32 \;\; 9/64]^T$,

$$\mathbf{C}_0 = \begin{bmatrix} b & e & d \\ 7/16 & 3/32 & 3/32 \\ 39/128 & 3/128 & 9/64 \end{bmatrix}, \; \mathbf{C}_1 = \begin{bmatrix} c & 0 & 0 \\ 3/32 & 0 & 0 \\ 39/128 & 3/128 & 1/128 \end{bmatrix}, \; \mathbf{C}_2 = \begin{bmatrix} c & 0 & d \\ 3/32 & 0 & 3/32 \\ 3/128 & 0 & 1/128 \end{bmatrix}.$$

Now, $\widetilde{M}$ is still not block circulant as promised, but close. Let $\omega = \exp(-i2\pi/3)$, $\mathbb{I}$ be the 3×3 identity matrix, and $\mathbf{1} = [1 \;\; 1 \;\; 1]^T$. Then the circulant part of $\widetilde{M}$ is block diagonalized by

$$F = \begin{bmatrix} \mathbb{I} & \mathbb{I} & \mathbb{I} \\ \mathbb{I} & \omega\mathbb{I} & \omega^2\mathbb{I} \\ \mathbb{I} & \omega^2\mathbb{I} & \omega^4\mathbb{I} \end{bmatrix}, \quad \text{i.e., } F^{-1} \begin{bmatrix} \mathbf{C}_0 & \mathbf{C}_1 & \mathbf{C}_2 \\ \mathbf{C}_2 & \mathbf{C}_0 & \mathbf{C}_1 \\ \mathbf{C}_1 & \mathbf{C}_2 & \mathbf{C}_0 \end{bmatrix} F = \begin{bmatrix} \mathbf{B}_0 & & \\ & \mathbf{B}_1 & \\ & & \mathbf{B}_2 \end{bmatrix}, \tag{2.6}$$

for some 3×3 matrices $\mathbf{B}_i$; by computation,

$$\mathbf{B}_0 = \begin{bmatrix} b+2c & e & 2d \\ \frac{5}{8} & \frac{3}{32} & \frac{3}{16} \\ \frac{21}{32} & \frac{3}{64} & \frac{5}{32} \end{bmatrix}, \; \mathbf{B}_1 = \begin{bmatrix} b-c & e & \frac{d}{2} - \frac{\sqrt{3}d}{2}i \\ \frac{11}{32} & \frac{3}{32} & \frac{3}{64} - \frac{3\sqrt{3}}{64}i \\ \frac{33}{256} + \frac{33\sqrt{3}}{256}i & \frac{3}{256} + \frac{3\sqrt{3}}{256}i & \frac{17}{128} \end{bmatrix}, \; \mathbf{B}_2 = \overline{\mathbf{B}_1}. \tag{2.7}$$

With $z = 1 - 3(s+t+u)$ and $a = 1 - b - 2(c+d) - e$, each row of M sums to 1, meaning that $[1 \; 1 \cdots 1]^T$ is an eigenvector of M associated with the eigenvalue 1. This, together with $1 + \omega + \omega^2 = 0$, implies that

$$\begin{aligned} &\begin{bmatrix} z & \mathbf{v}^T & \mathbf{v}^T & \mathbf{v}^T \\ \mathbf{w} & \mathbf{C}_0 & \mathbf{C}_1 & \mathbf{C}_2 \\ \mathbf{w} & \mathbf{C}_2 & \mathbf{C}_0 & \mathbf{C}_1 \\ \mathbf{w} & \mathbf{C}_1 & \mathbf{C}_2 & \mathbf{C}_0 \end{bmatrix} \begin{bmatrix} 1 & 0 & 0 & 0 \\ \mathbf{1} & \mathbb{I} & \mathbb{I} & \mathbb{I} \\ \mathbf{1} & \mathbb{I} & \omega\mathbb{I} & \omega^2\mathbb{I} \\ \mathbf{1} & \mathbb{I} & \omega^2\mathbb{I} & \omega^4\mathbb{I} \end{bmatrix} \\ &= \begin{bmatrix} 1 & 0 & 0 & 0 \\ \mathbf{1} & \mathbb{I} & \mathbb{I} & \mathbb{I} \\ \mathbf{1} & \mathbb{I} & \omega\mathbb{I} & \omega^2\mathbb{I} \\ \mathbf{1} & \mathbb{I} & \omega^2\mathbb{I} & \omega^4\mathbb{I} \end{bmatrix} \begin{bmatrix} 1 & 3\mathbf{v}^T & & \\ 0 & \mathbf{B}_0 - 3\mathbf{e}\mathbf{v}^T & & \\ & & \mathbf{B}_1 & \\ & & & \mathbf{B}_2 \end{bmatrix}. \end{aligned} \tag{2.8}$$

As such, we reduce M to a block diagonal matrix with one 4×4 and two 3×3 blocks. We refer to the 4×4 block as the 0th block, and $\mathbf{B}_i$, $i = 1, 2$, as the ith block.

We see that 1 is an eigenvalue of the 0th block. For convergence, it is necessary and sufficient that 1 is a simple eigenvalue. We denote the subdominant and sub-subdominant eigenvalues by λ and μ, so $1 > |\lambda| > |\mu|$.

An eigenvalue λ of M (and also of S) is said to have a *Fourier index* i if it "comes from" (i.e., it is also an eigenvalue of) the ith block. A multiple eigenvalue can have multiple Fourier indices. For simplicity, we assume that M will be constructed to have a real subdominant eigenvalue λ with geometric multiplicity 2 and a sub-subdominant eigenvalue $\mu = \lambda^2$ with geometric multiplicity 3; moreover,[3]

$$\mathcal{F}(\lambda) = \{1, 2\}, \quad \mathcal{F}(\lambda^2) = \{0, 1, 2\}. \tag{2.9}$$

Here $\mathcal{F}(\lambda)$ denotes the set of Fourier indices of the eigenvalue λ. We mention in passing that the first Fourier index condition is relevant to the injectivity of the characteristic map and the second is relevant to the curvature behavior in the vicinity of the extraordinary vertices; see [20, 21] for an in-depth theoretical development. While we do not need this part of the theory for our purpose, the above set of spectral conditions serves as a convenient guiding principle for our construction.

On the other hand, these spectral conditions alone are far from being sufficient for a scheme to be a flexible C^2 one. We recall the well-known C^1 and C^2 conditions in the next section.

2.2. Characteristic map and C^2 condition. Note that if $v \in \mathbb{R}^{19}$ is a set of scalar values assigned to the first three rings of the level 0 3-regular complex (as shown in Figure 4(a)), then according to our subdivision rules, the subdivision data on the first $2^j + 2$ rings of the level j 3-regular complex can be determined. Therefore, we obtain in the limit a subdivision function

$$f_v : D \to \mathbb{R}. \tag{2.10}$$

Here D is the 1-disc around the extraordinary vertex.

It is easy to see that every subdivision function satisfies the scaling relation

$$f_v(u) = f_{Sv}(2u) \quad \forall\, u \in \frac{1}{2}D. \tag{2.11}$$

In particular, if v is an eigenvector of S associated with an eigenvalue μ, then

$$f_v(u) = f_{\mu v}(2u) = \mu f_v(2u).$$

Despite the (rather artificial) way we embed D and the 3-regular complex into the plane as shown in Figure 4(a), one should not think of D as a subset of $\mathbb{R}^2$. That said, it is senseless to talk about the smoothness of f_v before we put a suitable differentiable structure on D (in differential geometry terms) or, equivalently, before we suitably parameterize f_v. On the other hand, since our subdivision scheme is based on a C^4 smooth box-spline, any subdivision function f_v is C^4 in the interior of each sector of D (assuming f_v is parameterized by the affine coordinates within each of the triangular sectors of D).

[3] These two conditions should be $\mathcal{F}(\lambda) = \{1, k-1\}$ and $\mathcal{F}(\lambda^2) = \{0, 2, k-2\}$ for a general valence k.

The standard way to parameterize subdivision functions is based on *characteristic maps*, due to Reif [24]. Assume that we have a subdivision scheme that satisfies the spectral properties around (2.9). Let u_1 and u_2 be two linearly independent eigenvectors associated with the subdominant eigenvalue λ. The characteristic map is given by

$$\chi = (f_{u_1}, f_{u_2}) : D \to \mathbb{R}^2. \tag{2.12}$$

If χ is *injective*, we can think of $\chi^{-1} : \chi(D) \to D$ as a parametrization of D. If χ is also *regular*, i.e., χ has a nonsingular Jacobian in the interior of each sector of D, then $f_v \circ \chi^{-1} : \chi(D) \to \mathbb{R}$ is C^1 smooth.

If we have a subdivision schemes that satisfies all the conditions above, except that all the eigenvalues smaller than λ are *strictly smaller* than λ^2 in modulus, then it is quite easy to show that all $f_v \circ \chi^{-1}$ are C^2 smooth. Such schemes are also easy to construct; the only problem is that they are not so useful since they produce limit functions with vanishing second derivatives *regardless of the initial data* and hence are not so interesting from an approximation or modeling point of view. A *flexible* C^2 scheme is one that is both C^2 and capable of producing all quadratic polynomials.

Going back to our original assumption that the sub-subdominant eigenvalue is exactly λ^2 with geometric multiplicity 3, let w_i, $i = 1, 2, 3$, be three linearly independent eigenvectors associated with λ^2. Then we have the following well-known result.

Theorem 2.1. *Such a subdivision scheme is a flexible C^2 one if*

$$\operatorname{span}\{f_{w_i} \circ \chi^{-1}(x_1, x_2) : i = 1, 2, 3\} = \operatorname{span}\{x_1^2, x_1 x_2, x_2^2\}. \tag{2.13}$$

This result is not specific to the valence 3 case. In fact, everything we have said so far is either directly applicable to or has a generalization to any valence $k \geqslant 3$.

The condition in Theorem 2.1 seems hard to satisfy and, as illustrated by Reif and Prautzsch's degree estimates [23, 25], is indeed hard to satisfy when $k > 3$. In the rest of this section, we establish the following.

Proposition 2.2 (main result). *The weights in Figure 3 can be chosen such that:*

(I) *the resulted characteristic map χ is the valence 3 Bers's chart [1, 7],*

(II) *the eigenfunctions corresponding to the sub-subdominant eigenvalues satisfy the flexible C^2 condition (2.13).*

2.3. Valence 3 Bers's chart. The valence k Bers' chart is a piecewise fractional power function: on the first sector of a k-gon it is given by the analytic map $z \mapsto z^{6/k}$, assuming that the first sector is affine transformed into the equilateral triangle bounded by $[0, 0]$, $[1, 0]$ and $[\cos(2\pi/3), \sin(2\pi/3)]$, followed by identifying this equilateral triangle with part of the complex plane. In the other $k - 1$ sectors, the chart is defined by rotational symmetry. It is not hard to check that these charts endow a triangle mesh with a conformal structure.

There is something special about the $k = 3$ case. First, the only $k \neq 6$ (and $\geqslant 3$) that makes $6/k$ an integer is $k = 3$. Moreover, we can identify the 3-gon D with the "projective regular hexagon," i.e., the regular hexagon with antipodal points identified, as shown in Figure 5(a)–(b). Then under this identification, the valence 3 Bers's chart is the *single* map $z \mapsto z^2$. This representation of the valence 3 Bers's chart will be very useful in section 2.7.

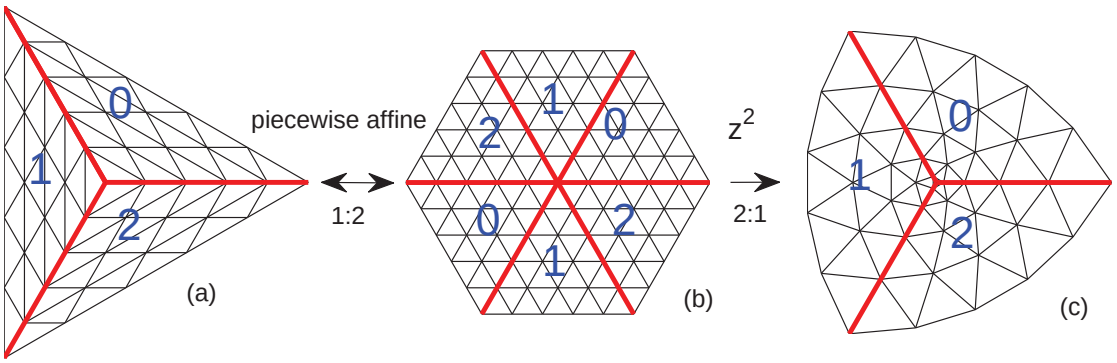

Figure 5. *A general valence k Bers's chart is defined piecewisely. The valence* 3 *Bers's chart, however, can be expressed by the* single *polynomial $z \mapsto z^2$ if we identify the* 3*-gon D with the "projective regular hexagon."*

2.4. Connection to Prautzsch and Reif's degree estimate. The valence 3 Bers's chart also gives a concrete illustration of how a key argument in Prautzsch and Reif's degree estimate breaks down in the valence 3 case. It is observed in [23] that if a valence k characteristic map consists of polynomial patches stitched together in a C^r fashion and the polynomial pieces are only of degree r, then the characteristic map must be 6-periodic (see Lemma 5.1 and Theorem 5.1 of [23]), which is, in general, impossible as the characteristic map must also be k-periodic. (As a result, the polynomial degree must, in general, be $\geqslant r+1$; this lower bound is further improved to $\geqslant 3r/2+1$ by a finer argument.) The only exception is when $k=3$, as illustrated by the valence 3 Bers's chart: it is both 3- and 6-periodic and consists only of polynomial patches of degree 2 stitched together in a C^∞ fashion away from the extraordinary point.

2.5. Shaping the spectrum. Since

$$\chi(u/2) = \frac{1}{4}\chi(u) \quad \forall u \in D, \tag{2.14}$$

in order to have a chance to satisfy Property (I) above we must force our scheme to have a subdominant eigenvalue $\lambda = 1/4$. So, according to the spectral conditions around (2.9), we need $\mathbf{B}_0 - 3ev^T$ to have $1/16$ as a simple dominant eigenvalue and $\mathbf{B}_1$, $\mathbf{B}_2$ to both have $1/4$ and $1/16$ as simple dominant and subdominant eigenvalues.

$\mathbf{B}_0$, $\mathbf{B}_1$, $\mathbf{B}_2$ only involve the 4 parameters (b,c,d,e), but $\mathbf{B}_0 - 3\,\mathbf{e}[s\ t\ u]$ involves all 7 parameters (b,c,d,e,s,t,u). By (2.7), $\mathbf{B}_1$ and $\mathbf{B}_2$ already have $1/16$ as one of their eigenvalues. If we set

$$b = c - 3d - 4e + 1/4, \tag{2.15}$$

then $\mathbf{B}_1$, and hence also $\mathbf{B}_2$, both have $1/4$ as an eigenvalue; moreover, the corresponding two eigenvectors of M (which uniquely determine the corresponding eigenvectors of S due to the block form in (2.1)) are independent of the parameters:

$$u_1 = \frac{1}{2}\Big[0,\ 2,\ -1,\ -1,\ 8,\ 3,\ -4,\ -6,\ -4,\ 3\Big]^T,\quad u_2 = \frac{\sqrt{3}}{2}\Big[0,\ 0,\ 1,\ -1,\ 0,\ 3,\ 4,\ 0,\ -4,\ -3\Big]^T. \tag{2.16}$$

Thanks to the Ferro–Tartaglia–Cardano formula and symbolic computation, we find that by further setting

$$s = [3/16 + 3(c - 2d - 5e + 8u + t) + 8(14dt + 6eu - 18ct + 24et - 3cu + 3du)]/ \\ [3 - 16(d + 3e)], \tag{2.17}$$

$\mathbf{B}_0 - 3ev^T$ has $1/16$ as an eigenvalue.

Therefore, after eliminating two of the seven parameters by (2.15) and (2.17), our subdivision matrix has the desired eigenvalues. As we shall see later, the C^2 condition specified by Theorem 2.1 will further take away two of the remaining 5 degrees of freedom, and then we have to choose the remaining 3 parameters in such a way that all the eigenvalues of M dependent of these parameters are $< 1/16$.

2.6. Relating valence 3 to valence 6. Everything presented in sections 2.1–2.2 is also applicable to any valence $\geqslant 3$, and, in particular, to valence $k = 6$. Let N_r be the number of vertices in the first r rings of the 3-regular complex, so $2N_r - 1$ is the corresponding number for the 6-regular complex. Corresponding to (2.1), we have a size $2N_3 - 1 = 37$ subdivision matrix S_6 in the case of valence $k = 6$ in the following block form:

$$S_6 = \begin{bmatrix} M_6 & 0 \\ A_6 & B_6 \end{bmatrix}, \tag{2.18}$$

where all three blocks are determined by the regular rules in (2); M_6 is of size $2N_2 - 1 = 19$. (We order the vertices on the 6-regular complex in a way similar to Figure 4(a).) Corresponding to (2.10), we have $F_{\widetilde{v}} : H \to \mathbb{R}$, where $\widetilde{v} \in \mathbb{R}^{2N_3-1}$ is any set of data on the first three rings of the 6-regular complex, H is the 1-disc (a regular hexagon) around the central vertex, and $F_{\widetilde{v}}$ is the corresponding subdivision function.

Figure 5(a)-(b) suggests a "doubling-up" operator from the 3-regular complex to the 6-regular complex; restricting this operator to the first r rings, we denote it by

$$\mathcal{D}_r : \mathbb{R}^{N_r} \to \mathbb{R}^{2N_r-1}.$$

The observation we need for proving Proposition 2.2 is the following.

Lemma 2.3. *If $\widetilde{u} \in \mathbb{R}^{2N_3-1}$ is such that $F_{\widetilde{u}}$ is a homogeneous polynomial p of degree 2ℓ, then*

1. *$\widetilde{u}$ is an eigenvector of S_6 associated with eigenvalue $2^{-2\ell}$,*
2. *$\widetilde{u} \in \text{range}(\mathcal{D}_3)$, so $u := \mathcal{D}_3^{-1}\widetilde{u}$ is well-defined, and*
3. *$F_{\widetilde{u}}$, being an even function, can be viewed as a function on the projective regular hexagon $H/\!\sim$. (Here, $\mathbf{x} \sim \mathbf{y} \Leftrightarrow \mathbf{x} = \pm\mathbf{y}$.)*

Furthermore, if (the parameters in M are chosen such that) $Su = 2^{-2\ell}u$, then

$$\mathbb{R} \leftarrow D : f_u = F_{\widetilde{u}} : H/\!\sim \to \mathbb{R} \tag{2.19}$$

if we identify D with $H/\!\sim$ (as in Figure 5.)

Proof. To appreciate the key idea in this lemma, first imagine that if we have an *arbitrary* vector $\widetilde{u}$ in range$(\mathcal{D}_3)$. We now subdivide $\widetilde{u}$ to the limit using the regular subdivision scheme operating on the 6-regular complex to get the limit function $F_{\widetilde{u}}$, and we subdivide $\mathcal{D}_3^{-1}\widetilde{u}$ to the limit using our subdivision scheme on the 3-regular complex to get f_u. Notice that the latter is based on a combination of the special valence 3 extraordinary vertex rule, used right at the vicinity of the valence 3 vertex, and the regular subdivision rule, used *away* from the valence 3 vertex, whereas the former has nothing to do with any extraordinary vertex rule. Therefore, even though the regular subdivision scheme has the right symmetry to guarantee that $F_{\widetilde{u}}$ is an even function (since $\widetilde{u} \in \text{range}(\mathcal{D}_3)$), there is no reason to expect that $f_u = F_{\widetilde{u}}$.

However, under the assumption that $Su = 2^{-2\ell}u$ and $S_6\widetilde{u} = 2^{-2\ell}\widetilde{u}$, then, together with the natural symmetries of S and S_6, the extraordinary vertex rule and the regular subdivision scheme have essentially the same action in the vicinity of the corresponding central vertices, more precisely,

$$\mathcal{D}_3 S^j u = S_6^j \widetilde{u} \quad \forall\, j = 0, 1, 2, \ldots.$$

Away from the central vertices, both rules are based on the regular rule, so all together we have $f_u = F_{\widetilde{u}}$. ∎

Due to the block forms (2.1) and (2.18), to specify the vector $\widetilde{u}$ (resp., u) in the lemma above, it is enough to specify its first $2N_2 - 1$ (resp., N_2) entries. Call this shorter vector $\widetilde{u}^s$; if $\widetilde{u}^s \neq 0$, then $\widetilde{u}$ is uniquely determined by

$$\widetilde{u} = \begin{bmatrix} \widetilde{u}^s \\ (2^{-2\ell} I - B_6)^{-1} A_6 \widetilde{u}^s \end{bmatrix}.$$

Notice that $\widetilde{u}^s \in \text{range}(\mathcal{D}_2)$. In the second half of the lemma above, we can actually weaken the assumption $Su = 2^{-2\ell}u$ to $M\mathcal{D}_2^{-1}\widetilde{u}^s = 2^{-2\ell}\mathcal{D}_2^{-1}\widetilde{u}^s$.

2.7. Proof of Proposition 2.2 and choice of parameters. We first prove Proposition 2.2(I) under only the condition (2.15). We shall only need condition (2.17) (and two new conditions on the parameters) when we deal with the C^2 conditions in Proposition 2.2(II).

The brute-force approach used in [30, Appendix B.7] can be applied here to prove (I). However, armed with Lemma 2.3, we can much more easily accomplish the task by checking that $\widetilde{u}_i := \mathcal{D}_2(u_i)$, $i = 1, 2$, are the (unique) data on the regular grid that generate the real and the imaginary parts of $z \mapsto z^2$ under the regular subdivision rule. Of course, the 6-regular grid, with coordinates denoted here by (x, y), can be identified with $\mathbb{Z}^2$, with coordinates denoted by (x_1, x_2), via a linear isomorphism,

$$\begin{bmatrix} x \\ y \end{bmatrix} = \begin{bmatrix} 1 & -1/2 \\ 0 & \sqrt{3}/2 \end{bmatrix} \begin{bmatrix} x_1 \\ x_2 \end{bmatrix},$$

so we are now back to the shift-invariant setting, and checking the polynomial reproduction condition above becomes a classical Strang–Fix-type calculation (a well-studied subject by itself.)

Using standard results in subdivision theory, any monomial of total degree $\leqslant 5$ can be written as a linear combination of the integer shifts of the three-directional box spline B_Ξ with subdivision mask (1.3). More precisely, if $\mu = (\mu_1, \mu_2)$, $|\mu| = \mu_1 + \mu_2 \leqslant 5$, then

$$x^\mu = \sum_{\alpha \in \mathbb{Z}^2} c_\alpha^\mu \, B_\Xi(x - \alpha), \tag{2.20}$$

where

$$c_\alpha^\mu = \sum_{\nu \leqslant \mu} \binom{\mu}{\nu} \alpha^\nu b_{\mu-\nu}, \tag{2.21}$$

and the b_μ, $|\mu| \leqslant 5$, are given by the following table:[4]

(2.22)

$\mu_1 \backslash \mu_2$	0	1	2	3	4	5
0	1	0	$-1/2$	0	$4/5$	0
1	0	$-1/4$	0	$2/5$	0	
2	$-1/2$	0	$2/5$	0		
3	0	$2/5$	0			
4	$4/5$	0				
5	0					

The real and imaginary parts of $z \mapsto z^2$ are

$$x^2 - y^2 = x_1^2 - x_1 x_2 - x_2^2/2, \quad 2xy = \sqrt{3}(x_1 x_2 - x_2^2/2). \tag{2.23}$$

Using (2.20)–(2.22),[5] it is straightforward to check that $\widetilde{u}_1$ and $\widetilde{u}_2$ are the unique vectors that generate these two degree 2 homogeneous polynomials on the x_1-x_2 plane. This verifies (I).

For (II) (the C^2 conditions), we need to force the sub-subdominant eigenvectors of M, w_i, $i = 1, 2, 3$, after "doubling-up," to be the unique initial data that generate, under the regular subdivision rule, the following homogeneous degree 4 polynomials:

$$\begin{aligned} (x^2 - y^2)^2 &= x_1^4 - 2x_1^3 x_2 + x_1 x_2^3 + x_2^4/4, \\ (x^2 - y^2)(2xy) &= \sqrt{3}(x_1^3 x_2 - 3x_1^2 x_2^2/2 + x_2^4/4), \\ (2xy)^2 &= 3x_1^2 x_2^2 - 3x_1 x_2^3 + 3x_2^4/4. \end{aligned} \tag{2.24}$$

By calculations based on (2.20)–(2.22), we demand M in (2.1) to have the following three eigenvectors associated with eigenvalue $1/16$:

$$\begin{aligned} w_1 &= \frac{1}{20}\Big[12,\ 2,\ -13,\ -13,\ 212,\ -33,\ -28,\ 102,\ -28,\ -33\Big]^T, \\ w_2 &= \frac{\sqrt{3}}{4}\Big[0,\ 0,\ -1,\ 1,\ 0,\ 9,\ -16,\ 0,\ 16,\ -9\Big]^T, \\ w_3 &= \frac{1}{20}\Big[12,\ -18,\ -3,\ -3,\ -108,\ 57,\ 132,\ -78,\ 132,\ 57\Big]^T. \end{aligned} \tag{2.25}$$

Condition (2.17) is only enough to guarantee that M has $1/16$ as a triple eigenvalue but not enough to guarantee the above eigenvector condition. After imposing conditions (2.15) and

[4] These b_μ are computed recursively by the formula: $b_{(0,0)} = 1$, $b_\mu = \sum_{0 \neq \nu \leqslant \mu} \binom{\mu}{\nu} 2^{|\mu-\nu|} b_{\mu-\nu} [(-iD)^\nu \widehat{\mathbf{a}}](0)(1 - 2^{|\mu|}\widehat{\mathbf{a}}(0))^{-1}$, where $\widehat{\mathbf{a}}(\omega) = \sum_\alpha a(\alpha) e^{-i\alpha\cdot\omega}/4$. One can verify the values of b_μ in the table using this formula and (1.3).

[5] For a more elementary, but more tedious, approach, one can work out the piecewise (degree 7) polynomial representation of the box-spline B_Ξ based on (1.2) and use it to work out how to reproduce any polynomial of total degree $\leqslant 5$.

(2.17), M has five remaining parameters. After representing $M[w_1\ w_2\ w_3] - [w_1\ w_2\ w_3]/16$ in terms of these five parameters (c, d, e, t, u), we find that two extra linear conditions,

$$c = 9/64 + 3e, \quad d = 1/64 + e, \tag{2.26}$$

are enough to guarantee that all entries in $M[w_1\ w_2\ w_3] - [w_1\ w_2\ w_3]/16$ are zeros.

Note that conditions (2.15) and (2.26) are linear but (2.17) is not. However, (2.26) and (2.17) together imply that

$$s = 3/16 + 2t,$$

so all the weights in our extraordinary vertex rule (Figure 3) are linearly dependent on the three parameters (e, t, u). This is bound to happen as the overall conditions imposed on M are, after all, linear:

$$M[u_1, u_2, w_1, w_2, w_3] = [u_1, u_2, w_1, w_2, w_3]\ \mathrm{diag}([1/4, 1/4, 1/16, 1/16, 1/16]).$$

We could have directly used the above to work out the same results; we just happened to go through the devious path of first working out conditions on the parameters *just* to satisfy the eigenvalue conditions (which are nonlinear and are of interest by themselves), before imposing the eigenvector conditions.

We must still verify that the remaining three parameters (e, t, u) can be chosen such that all the remaining eigenvalues are strictly less than $1/16$ in modulus. Only four eigenvalues of M are dependent on (e, t, u), and they are $15/128 - 7e$ (repeated twice) and

$$1/8 + e - 9t/2 - 3u/2 \pm \sqrt{13 + 16(8e - 30t - 33u) + 256(4e^2 + 81t^2 + 9u^2 - 84et + 12eu + 54ut)}/32.$$

It can be shown analytically that these eigenvalues are smaller than $1/16$ in modulus if and only if (e, t, u) lies in a small bounded open subset of the first octant of the e-t-u space. A natural choice would be the unique set of parameters that vanish all four eigenvalues, namely,

$$e = 15/896,\ t = 295/19264, \quad u = 1403/28896.$$

This leads to the positive subdivision weights in the caption of Figure 3, and the Jordan blocks corresponding to the four zero eigenvalues are $\left(\begin{smallmatrix} 0 & 1 \\ 0 & 0 \end{smallmatrix}\right)$ and $\left(\begin{smallmatrix} 0 & 0 \\ 0 & 0 \end{smallmatrix}\right)$. This is the only defective eigenvalue of the subdivision matrix S, a fact to be used in the evaluation algorithm described in section 3.1. ∎

3. Applications. In the introduction section, we mentioned the application of subdivision surfaces, developed in [5], in solving the Canham–Helfrich–Evans model (1.1). The idea is to approximate the sought-for surface by a subdivision surface. A subdivision surface is specified by a control mesh $M = (\mathcal{V}, \mathcal{F})$, where $\mathcal{V} \in \mathbb{R}^{\#V \times 3}$ records the three-dimensional coordinates of the vertices of the control mesh, $\#V$ denotes the total number of vertices, and $\mathcal{F} \in \mathcal{I}^{\#F \times 3}$ is a list of triplets of indices from $\mathcal{I} := \{1, \ldots, \#V\}$ which records the bounding vertices of each of the $\#F$ triangle faces in the mesh M. We assume that the mesh realizes a closed simplicial surface.

Surfaces with genus 0 or 1 can be triangulated in such a way that only valence 3 and 6 vertices are involved; see Figure 6. (Conversely, it can be shown by Euler's relation that

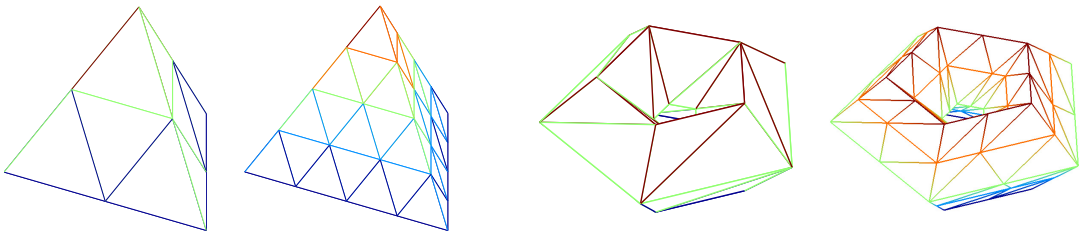

(a) genus 0 (spherical): $\mathcal{F}_{\text{tetra},1}$ & $\mathcal{F}_{\text{tetra},2}$ (b) genus 1 (toroidal)

Figure 6. *Left* 2 *panels: Genus* 0 *surfaces with only valence* 3 *and* 6 *vertices (subdivided tetrahedra). Right* 2 *panels: (*4×5 *and* 8×10*) regularly triangulated tori, with only valence* 6 *vertices.*

the closed surfaces that are modelled with only valence 3 and 6 vertices must be of genus 0 or 1.) The special scheme developed in this paper can then be applied to numerically solve the Canham–Helfrich–Evan problem in the genus 0 and 1 cases by *fixing* $\mathcal{F}$ to be one of the genus 0 or 1 triangulation as in Figure 6 and *varying* $\mathcal{V} \in \mathbb{R}^{\#V\times 3}$ by a nonlinear optimization solver. As such, we solve the following finite-dimensional nonlinear optimization problem as an approximation to (1.1):

$$\min_{\mathcal{V}\in\mathbb{R}^{\#V\times 3}} \overbrace{\int_{S[\mathcal{V}]} H^2\, dA}^{=:W(\mathcal{V})} \text{ s.t. } \begin{cases} \text{(i)} & A(\mathcal{V}) := \int_{S[\mathcal{V}]} 1\, dA = A_0, \\ \text{(ii)} & V(\mathcal{V}) := \frac{1}{3}\int_{S[\mathcal{V}]} [x\hat{\mathbf{i}} + y\hat{\mathbf{j}} + z\hat{\mathbf{k}}]\cdot\hat{\mathbf{n}}\, dA = V_0, \\ \text{(iii)} & M(\mathcal{V}) := \int_{S[\mathcal{V}]} H\, dA = M_0. \end{cases} \tag{3.1}$$

In above, $S[\mathcal{V}]$ is the subdivision surface determined by $\mathcal{V}$ (and the fixed $\mathcal{F}$.)

We shall use the notation $(V, \mathcal{F}_{\text{tetra}})$ to denote a tetrahedral control mesh as in Figure 6(a). The connectivity information encoded in $\mathcal{F}_{\text{tetra}}$ defines what is usually called an abstract simplicial complex. We also use the notation $\mathcal{F}_{\text{tetra},j}$ to denote the complex of a j-times subdivided tetrahedron.

We refer to problem (3.1) simply as a Helfrich problem and the same problem without constraint (iii) as a Canham problem. In Figure 7 we give an example of the numerical solution of a Canham problem;[6] it illustrates that the C2g0 scheme, being a higher order scheme than the Loop scheme, can potentially approximates a surface more accurately.

3.1. Evaluation algorithm. In order to compute the various quantities of interest pertaining to a subdivision surface, e.g., mean and Gauss curvatures, $W(\mathcal{V})$, $A(\mathcal{V})$, $V(\mathcal{V})$, $M(\mathcal{V})$ in the Helfrich model, and the harmonic energy in the next section, we need to be able to evaluate the surface parametrizations and their derivatives efficiently. For this purpose, we adapt the idea from Stam [28]. Since we consider only closed triangle meshes with valence 3 and 6 vertices, there are three types of triangles to handle:

- [Type-0 triangle] These are triangles with valence 6 bounding vertices, and all vertices adjacent to the three bounding vertices also have valence 6. See Figure 8. In this case,

[6] We use the solver fmincon() in the MATLAB optimization toolbox, which requires one to input an initial guess, and function handles for computing the objective (W) and constraint functions (A, V, M), as well as their gradients. See [5] and also the related article [9]. A few related problems (see Remark 3.1 and (3.12)) in the rest of the paper are solved using the same solver.

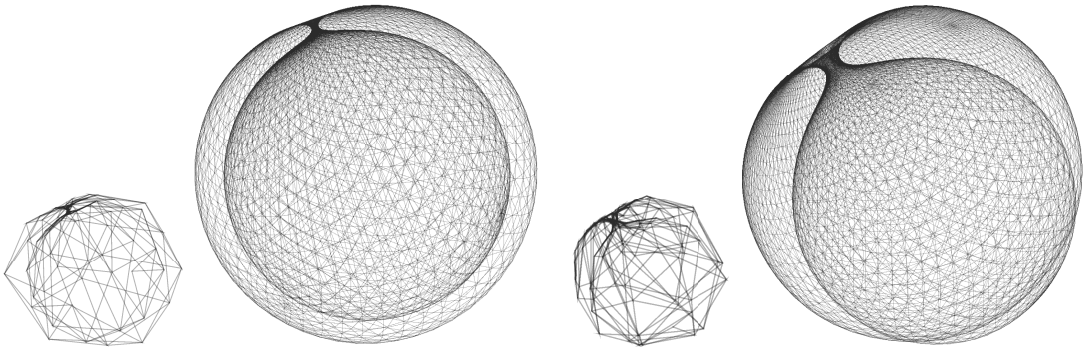

(a) C2g0 (Willmore energy = 25.125) (b) Loop (Willmore energy = 25.303)

Figure 7. *Numerical solutions of the Canham problem with reduced volume* $v_0 = 0.18$. (a) *using the C2g0 scheme and* (b) *using the Loop scheme. In both cases, the control mesh is based on* $\mathcal{F}_{\text{tetra},3}$ *(with* 130 *vertices). The resulted control mesh (left) is subdivided three more times and displayed (right). It is believed that the true solution approaches a double sphere with a catenoid-like neck when* $v_0 \to 0$. *The Loop scheme gives a surface with self-intersection, while the C2g0 scheme produces a double sphere without self-intersection.*

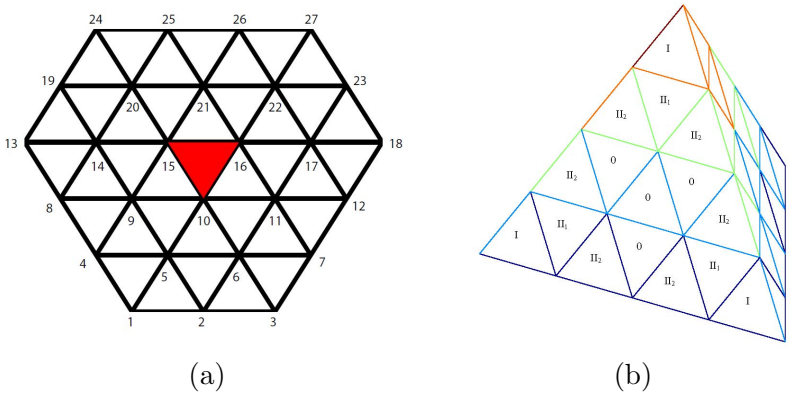

(a) (b)

Figure 8. (a) *Type-*0 *configuration,* (b) *types of triangle in a twice subdivided tetrahedron.*

the surface patch is determined by the surrounding 27 control vertices and the surface parametrization[7] $\mathbf{s}(v,w) = [X(v,w), Y(v,w), Z(v,w)]^T$ is a *single* degree 7 polynomial function in each component and can be evaluated as

$$\mathbf{s}(v,w) = \mathbf{c}^T Q b(v,w), \tag{3.2}$$

where $b(v,w)$ is a length 36 column vector consisting of any ordered basis of the space of bivariate polynomials of total degree 7 (we use the Bernstein–Bézeir basis $\{\frac{7!}{i!j!k!}u^i v^j w^k : i+j+k=7\}$), Q is a suitable 27×36 matrix (dictated by the underlying three-directional box-spline and the choice of ordered polynomial basis), and $\mathbf{c}$ is the 27×3 array of control vertices around the type-0 triangle ordered according to Figure 8(a).

[7]Here and below, the (v,w) parameters live in the reference triangle $\Omega := \{(v,w) : v \in [0,1] \text{ and } w \in [0, 1-v]\}$. As such, the barycentric coordinates of (v,w) are $(u = 1-v-w, v, w)$.

- [Type-II triangle] These are triangles with valence 6 bounding vertices, but one of them has an adjacent vertex with valence 3.[8] In this case, the surface parametrization for each component is a potentially different degree 7 polynomial on each of the *four* subtriangles of Ω when we midpoint subdivide Ω. The evaluation algorithm is similar to that of type-0, except that for each of the four subtriangles of Ω we need to add an extra linear map that maps the control vertices around the type-II triangle to the 27 control vertices that determine the polynomial piece defined on that subtriangle.
  There are two subtypes among the type-II faces: those that are on the side (labelled "II_1" in Figure 8(b)) and those that are in the middle (labelled "II_2"); these two subtypes of surface patches are determined by 23 and 21 control vertices, respectively.
- [Type-I triangle] These are triangles with one valence 3 bounding vertex and the other two being valence 6. In this case, the surface patch is determined by 18 surrounding control vertices,[9] and the surface parametrization consists of an *infinite* number of degree 7 polynomial pieces in each component. (In the subdivision surface literature, these are called *infinite spline rings*.) In this case each component of the parametrized surface $\mathbf{s}(v,w) = [X(v,w), Y(v,w), Z(v,w)]^T$, $(v,w) \in \Omega$, is a piecewise polynomial with infinite pieces, and there appears to be no convenient, constant time way to evaluate $p(v,w)$ for arbitrary parameter values v, w. This is where Stam's idea comes in, based on exploiting linearity and stationarity. If $\mathbf{c}$ is the 18×3 array of control vertices around a type-I triangle, and if we decompose $\mathbf{c}$ in the (generalized) eigen-basis of the subdivision matrix S_{trim} (see footnote 9), $\mathbf{c} = \sum_{i=1}^{18} v_i \hat{\mathbf{c}}_i$, then the parametrization can be written as

$$\mathbf{s}(v,w) = \sum_{i=1}^{18} \hat{\mathbf{c}}_i^T \hat{b}_i(v,w), \tag{3.3}$$

  where $\hat{b}_i(v,w)$ is an "eigen-subdivision function," i.e., the subdivision limit given by the "eigen-control data" v_i. The observation is that, while $\mathbf{s}(v,w)$ seems hard to evaluate, each $\hat{b}_i(v,w)$ is easier to evaluate because it is either "self-similar" in the sense of $\hat{b}_i(v/2, w/2) = \lambda_i \hat{b}_i(v,w)$ when $S_{\text{trim}} v_i = \lambda_i v_i$ (v_i is an eigenvector), or $\hat{b}_i(v/2, w/2) = \hat{b}_{i-1}(v,w) + \lambda_i \hat{b}_i(v,w)$ when $S_{\text{trim}} v_i = v_{i-1} + \lambda_i v_i$ (v_i is a generalized eigenvector.) In the former case, $\hat{b}_i(v,w)$ is determined by its values on the "outer wedge" $\Omega_1^1 \cup \Omega_2^1 \cup \Omega_3^1$ of Ω (see Figure 9), and for each $k = 1,2,3$, $\hat{b}_i|\Omega_k^1$ in turn has the structure of a type-II_ℓ patch, $\ell = 1$ when $k = 1,3$ and $\ell = 2$ when $k = 2$, so can be evaluated accordingly. The latter case is handled similarly.

As the discussion above suggests, the implementation of type-I triangles depends on that of type-II triangles, which in turn depends on that of type-0 triangles. See our MATLAB implementation Evaluate$_C$2g0.m, available at http://www.math.drexel.edu/~tyu/C2g0.

[8] We assume that the valence 3 vertices are isolated enough that when this happens exactly one of the three bounding vertices will have exactly one valence 3 adjacent vertex. In the case of a tetrahedron, subdividing it twice will guarantee this property.

[9] If the type-I triangle is the one bounded by vertices 1,2,3 in Figure 4(a), then the 18 control vertices that determine the patch are the 19 vertices there with vertex 17 excluded. We also define the corresponding trimmed subdivision matrix $S_{\text{trim}} \in \mathbb{R}^{18\times 18}$ as the matrix $S \in \mathbb{R}^{19\times 19}$ in (2.1)-(2.3) with the 17th row and column removed.

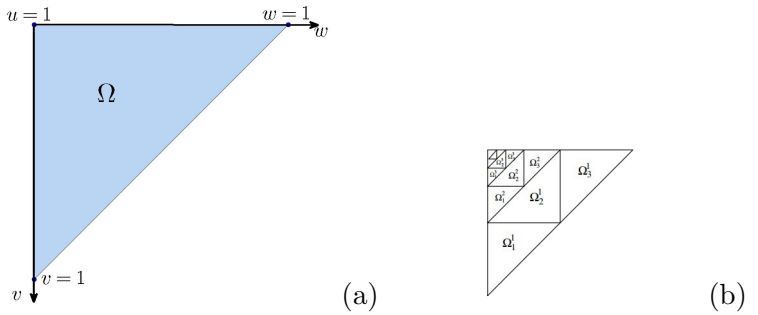

Figure 9. (a) *The parameter domain* Ω (b) *Partition of* Ω.

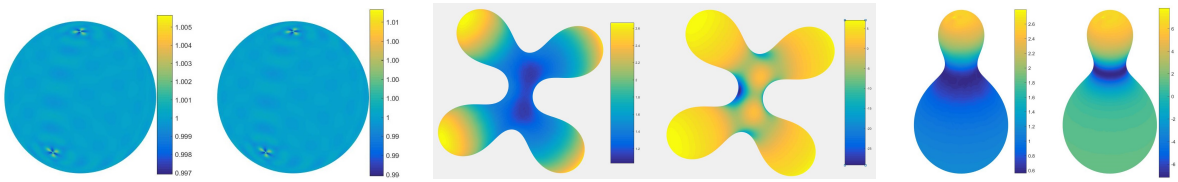

(a) almost round sphere (b) H-shaped starfish (c) pear

Figure 10. *Mean and Gauss curvature plots of three C2g0 subdivision surfaces. The control vertices* $\mathcal{V}$ *are obtained by solving a Helfrich problem (c.f. Figure 1) with* $\mathcal{F} = \mathcal{F}_{\text{tetra},3}$ *in* (a) *&* (c) *and* $\mathcal{F}_{\text{tetra},4}$ *in* (b).

A standard use of such an evaluation algorithm is the computation of the first and second fundamental forms based on the following formulas:

$$I = \begin{bmatrix} E{=}\langle \mathbf{s}_v, \mathbf{s}_v \rangle & F{=}\langle \mathbf{s}_v, \mathbf{s}_w \rangle \\ F{=}\langle \mathbf{s}_w, \mathbf{s}_v \rangle & G{=}\langle \mathbf{s}_w, \mathbf{s}_w \rangle \end{bmatrix}, \quad II = \begin{bmatrix} e{=}\langle \mathbf{n}, \mathbf{s}_{vv} \rangle & f{=}\langle \mathbf{n}, \mathbf{s}_{vw} \rangle \\ f{=}\langle \mathbf{n}, \mathbf{s}_{wv} \rangle & g{=}\langle \mathbf{n}, \mathbf{s}_{ww} \rangle \end{bmatrix}, \quad \mathbf{n} = \mathbf{s}_v \times \mathbf{s}_w / \|\mathbf{s}_v \times \mathbf{s}_w\|. \tag{3.4}$$

In Figure 10, we give examples of Gauss ($K = \det(I^{-1}II)$) and mean curvature ($H = 1/2 \operatorname{trace}(I^{-1}II)$) plots for some genus 0 surfaces generated using the evaluation algorithm. Here the normal vector $\mathbf{n}$ points inward, so that $H \equiv 1$ for the unit sphere.

For our purposes, it is important to note that for any face f in the triangle mesh, the parametric surface patch can be written as

$$\mathbf{s} = \mathbf{s}_f = \mathbf{c}_f^T \mathbf{b}^{\text{type}(f)}, \quad \text{type}(f) \in \{0, \text{II}_1, \text{II}_2, \text{I}\}, \tag{3.5}$$

where $\mathbf{c}_f$ is formed by selecting the right set of rows from $\mathcal{V}$, whereas $\mathbf{b}^{\text{type}(f)}$ is a vector of functions *independent* of $\mathcal{V}$. For a type-0 face f, this relation is given by (3.2). For a type-I face f, we write (3.3) in matrix form as $\mathbf{s} = \hat{\mathbf{c}}\hat{\mathbf{b}}$, $V\hat{\mathbf{c}} = \mathbf{c}_f$ with $V = [v_1, \cdots, v_{18}]$ the matrix of (generalized) eigenvectors of S_{trim}, and then $\mathbf{s}_f = (V^{-1}\mathbf{c}_f)^T\hat{\mathbf{b}} = \mathbf{c}_f^T(V^{-T}\hat{\mathbf{b}})$, which is now in the desired form (3.5). Type-II patches are treated similarly.

When various geometric functionals of the subdivision subdivision surface and their gradients have to be computed for *many different* $\mathcal{V}$ *but the same* $\mathcal{F}$, it is economical to *precompute* the basis functions $\mathbf{b}^{\text{type}(f)}$, $\text{type}(f) \in \{0, \text{II}_1, \text{II}_2, \text{I}\}$ at quadrature points. The same precomputation also facilities a parallel implementation of these functionals and their gradients [5]. Below, we shall see how (3.5) is used in the computation of the gradient of harmonic energy.

3.2. Harmonic energy. The harmonic energy, Dirichlet energy, or simply energy of a C^1 map $\varphi : \mathcal{M} \to \mathcal{N}$ between Riemannian manifolds $(\mathcal{M}, g)$ and $(\mathcal{N}, h)$ is defined by

$$\mathcal{E}[\varphi] = \int_{\mathcal{M}} \|d\varphi\|^2 d\mathcal{M}, \tag{3.6}$$

where $d\mathcal{M}$ is the volume form of $(\mathcal{M}, g)$, and the energy density $\|d\varphi\|^2$ at any $x \in \mathcal{M}$ is the Hilbert–Schmidt norm of $d\varphi_x : (T_x\mathcal{M}, \langle , \rangle_g) \to (T_{\varphi(x)}\mathcal{N}, \langle , \rangle_h)$, i.e.,

$$\|d\varphi_x\|^2 = \mathrm{trace}_{g,h}(d\varphi_x{}^* d\varphi_x) = \sum_i \langle d\varphi_x{}^* d\varphi_x\, e_i, e_i\rangle_g = \sum_i \langle d\varphi_x\, e_i, d\varphi_x\, e_i\rangle_h \tag{3.7}$$

for any orthonormal basis (e_i) in $(T_x\mathcal{M}, \langle , \rangle_g)$. See [15, Chapter 8].[10] Such a map is called harmonic if it is a critical point of $\mathcal{E}$. When $\mathcal{M}$ is two-dimensional, two "accidents" happen:

(i) The energy does not depend on the exact Riemannian metric on $\mathcal{M}$ but only its conformal class.

(ii) If furthermore $\mathcal{M}$ is of genus 0, then every harmonic map is conformal.

To see why (i) is specific to surfaces, under a conformal change of metric $\tilde{g}_{i,j}(x) = \lambda(x)^2\, g_{i,j}(x)$ the area form $d\mathcal{M} = \sqrt{\det(g_{i,j})}\, dx^1 \wedge dx^2$ transforms as $d\tilde{\mathcal{M}} = \sqrt{\det(\tilde{g}_{i,j})}\, dx^1 \wedge dx^2 = \sqrt{\lambda^{2(\dim \mathcal{M})}\det(g_{i,j})}\, dx^1 \wedge dx^2 = \lambda^2\, d\mathcal{M}$ when $\dim \mathcal{M} = 2$, whereas the energy density transforms as $\mathrm{trace}_{\tilde{g},h}(d\varphi_x{}^* d\varphi_x) = \lambda(x)^{-2}\, \mathrm{trace}_{g,h}(d\varphi_x{}^* d\varphi_x)$ regardless of $\dim \mathcal{M}$. As such, $\mathcal{E}[\varphi]$ is independent of λ, hence (i), when and only when $\dim(\mathcal{M}) = 2$. For (ii), see [15, Chapter 9].

If we endow the spherical or toroidal triangle mesh in Figure 6 with the conformal structure based on the valence 3 and 6 Bers's charts, recall Figure 5, then a Riemann surface $\mathcal{M}$ results. Moreover, the subdivision functions $\varphi : \mathcal{M} \to \mathbb{R}^3$ produced by the C2g0 scheme are, according to Theorem 2.1, more than regular enough to possess a well-defined energy $\mathcal{E}[\varphi]$.

3.3. Computing harmonic energy. We describe how to compute $\mathcal{E}[\varphi]$ and its gradient vector with respect the control vertices $\mathcal{V}$. We focus on the spherical case as this is our main interest. The torodial case is only easier as there are only valence six vertices.

We continue to use the notation $\mathcal{M} := \mathcal{M}(\mathcal{F}_{\mathrm{tetra}})$ to denote the Riemann surface after we endow the (abstract) simplicial complex specified by $\mathcal{F}_{\mathrm{tetra}}$ with Bers's conformal structure. With $\mathcal{F}_{\mathrm{tetra}}$ and $\mathcal{M}$ now fixed, it is the data in $\mathcal{V}$ that determines the subdivision map

$$\varphi := \varphi_{\mathcal{V}} : \mathcal{M} \to \mathbb{R}^3.$$

We overload notation and write

$$\mathcal{E}(\mathcal{V}) := \mathcal{E}[\varphi_{\mathcal{V}}], \text{ and } \nabla\mathcal{E}(\mathcal{V})$$

for the gradient vector of $\mathcal{E}$, now viewed as a function from $\mathbb{R}^{\#V\times 3}$ to $\mathbb{R}$, at $\mathcal{V}$.

[10] The exposition in [15, Chapter 8] does not appeal to what operator theorists call the Hilbert–Schmidt norm. In differential geometry parlance, (3.7) is equivalent to taking the pullback by φ of the metric tensor of N, then identifying it as a linear operator on $T_x\mathcal{M}$ (this identification is based on the metric on $\mathcal{M}$), followed by taking the trace of the operator. Regarding the notation $\mathrm{trace}_{g,h} d\varphi_x{}^* d\varphi_x$ in (3.7), the trace of a linear map from $T_x\mathcal{M}$ to itself does not depend on any inner product (nor basis); it is the definition of $d\varphi_x{}^* d\varphi_x$ that relies on both the Riemannian metrics on M and N.

Our algorithm for computing $\mathcal{E}(\mathcal{V})$ and $\nabla\mathcal{E}(\mathcal{V})$ is based on writing the integral (3.6) as a sum over all the type-0, I, and II faces in $\mathcal{F}_{\text{tetra}}$ (recall Figure 8(b)),

$$\mathcal{E}(\mathcal{V}) = \sum_{f\in\mathcal{F}_{\text{tetra}}} \int_f \|d\varphi\|^2 d\mathcal{M}. \tag{3.8}$$

For each face $f \in \mathcal{F}_{\text{tetra}}$, there is a vector of control vertices that determines the surface patch $\varphi_{\mathcal{V}}|_f$. In section 3.1, f is always identified with the reference triangle Ω (recall Figure 9), and $\varphi_{\mathcal{V}}|_f$ is written as $\mathbf{s}_f : \Omega \to \mathbb{R}^3$ there. However, this identification distorts the angles specified by the conformal structure on f. To compute the integral in (3.8) correctly, let $\tau = \left(\begin{smallmatrix} 1 & -1/\sqrt{3} \\ 0 & 2/\sqrt{3} \end{smallmatrix}\right)$, and then $\tau^{-1}\Omega$ is an equilateral triangle. Define $\tilde{\mathbf{s}}_f = \mathbf{s}_f \circ \tau$, so $d\tilde{\mathbf{s}}_f = d\mathbf{s}_f|_\tau.\tau$ (as a 3×2 matrix), and

$$\begin{aligned}\int_{[f]} \|d\varphi\|^2 d\mathcal{M} &= \int_{\tau^{-1}\Omega} \operatorname{trace}(d\tilde{\mathbf{s}}_f^T d\tilde{\mathbf{s}}_f)\, d\tilde{v}\, d\tilde{w} = \int_\Omega \operatorname{trace}(\tau^T I \tau)\det(\tau^{-1}) dv\, dw \\ &= \frac{2}{\sqrt{3}} \int_\Omega \langle \mathbf{s}_{f,v}, \mathbf{s}_{f,v}\rangle - \langle \mathbf{s}_{f,v}, \mathbf{s}_{f,w}\rangle + \langle \mathbf{s}_{f,w}, \mathbf{s}_{f,w}\rangle\, dv\, dw,\end{aligned} \tag{3.9}$$

where I is the first fundamental form in (3.4). Since the integrand can be evaluated using the algorithm developed in section 3.1, the integral can then be computed based on a numerical quadrature.

This algorithm can be parallelized over the faces; see [4, 5].

To compute $\nabla\mathcal{E}(\mathcal{V})$ both sequentially and in parallel, we again use the strategy developed in [4, 5]. In the case at hand, it is based on the fact that every patch of a subdivision surface can be expressed in the form (3.5). Write $\mathcal{E}_0(\mathbf{c}_f)$, $\mathcal{E}_{\text{II}_1}(\mathbf{c}_f)$, $\mathcal{E}_{\text{II}_2}(\mathbf{c}_f)$, $\mathcal{E}_{\text{I}}(\mathbf{c}_f)$ for the integrals in (3.8)–(3.9) when $\text{type}(f) = 0, \text{II}_1, \text{II}_2, \text{I}$, respectively; these are viewed as functions

$$\mathcal{E}_0 : \mathbb{R}^{27\times 3} \to \mathbb{R},\quad \mathcal{E}_{\text{II}_1} : \mathbb{R}^{23\times 3} \to \mathbb{R},\quad \mathcal{E}_{\text{II}_2} : \mathbb{R}^{21\times 3} \to \mathbb{R},\quad \mathcal{E}_{\text{I}} : \mathbb{R}^{18\times 3} \to \mathbb{R},$$

and we shall compute their gradients in (3.11).[11] The (local) control vertices $\mathbf{c}_f$ is related to the (global) vertex list $\mathcal{V}$ via a projection: $P_f\mathcal{V} = \mathbf{c}_f$. P_f can be regarded as a "global to local map" that picks out the rows from $\mathcal{V}$ that contribute to the surface $\mathbf{s}_f$. This matrix P_f is not to be formed in actual computation, but it put the energy functional in a form in which the chain rule can be applied:

$$\underbrace{\nabla\mathcal{E}(\mathcal{V})}_{\text{global gradient}} = \sum_{f\in\mathcal{F}} \underbrace{P_f^T}_{\substack{\text{local to}\\ \text{global}\\ \text{map}}} \underbrace{\nabla\mathcal{E}_{\text{type}(f)}(\mathbf{c}_f)}_{\text{local gradient}}. \tag{3.10}$$

It remains to work out an expression for the local gradient vector $\nabla\mathcal{E}_{\text{type}(f)}(\mathbf{c}_f)$. In virtue of (3.5), the algebra is the same for each type, say, $\text{type}(f) = \text{I}$, by (3.9)

$$\begin{aligned}\nabla\mathcal{E}_{\text{I}}(\mathbf{c}_f) &= \frac{2}{\sqrt{3}} \int_\Omega \nabla\langle \mathbf{c}_f^T\mathbf{b}_v^{\text{I}}, \mathbf{c}_f^T\mathbf{b}_v^{\text{I}}\rangle - \nabla\langle \mathbf{c}_f^T\mathbf{b}_v^{\text{I}}, \mathbf{c}_f^T\mathbf{b}_w^{\text{I}}\rangle + \nabla\langle \mathbf{c}_f^T\mathbf{b}_w^{\text{I}}, \mathbf{c}_f^T\mathbf{b}_w^{\text{I}}\rangle\, dv\, dw \\ &= \frac{2}{\sqrt{3}} \int_\Omega \left[2\mathbf{b}_v^{\text{I}}(\mathbf{b}_v^{\text{I}})^T - \mathbf{b}_v^{\text{I}}(\mathbf{b}_w^{\text{I}})^T - \mathbf{b}_w^{\text{I}}(\mathbf{b}_v^{\text{I}})^T + 2\mathbf{b}_w^{\text{I}}(\mathbf{b}_w^{\text{I}})^T\right]\mathbf{c}_f\, dv\, dw.\end{aligned} \tag{3.11}$$

[11] We write the gradients of $\mathcal{E}_{\text{type}(f)}(\mathbf{c}_f)$ (resp., $\mathcal{E}(\mathcal{V})$) as a matrix with the same dimensions as $\mathbf{c}_f$ (resp., $\mathcal{V}$). This way the matrix products in (3.10) and (3.11) are valid.

The same formula holds with "I" replaced by "0," "II_1," or "II_2."

For the parallel implementation based on (3.10)–(3.11), see [4, 5], and also the CUDA implementation provided in http://www.math.drexel.edu/~tyu/C2g0.

Remark 3.1. How big should we expect $\mathcal{E}(\mathcal{V})$ to be? There is only one conformal structure on the sphere, so as a Riemann surface our $\mathcal{M}(\mathcal{F}_{\text{tetra}})$ is no different from the unit sphere in three-space with the conformal structure inherited from $\mathbb{R}^3$. Now consider the identity map from S^2 to itself, which has energy $2 \cdot \text{area}(S^2) = 8\pi$. Using the numerical tools we have developed, we solve the following problem: $\min_{\mathcal{V}\in\mathbb{R}^{\#V\times 3}} \mathcal{E}(\mathcal{V})$, s.t. $A(\mathcal{V}) = 4\pi$, the numerical solution quickly converges to a map with energy equals $25.13274 \approx 8\pi$ for both $\mathcal{F} = \mathcal{F}_{\text{tetra},3}$ and $\mathcal{F}_{\text{tetra},4}$. We suspect that whenever a genus 0 surface is parametrized over the Riemann sphere has area normalized to 4π, the energy of the parametrization map is at least 8π.

3.4. Regularizing parameterization via harmonic energy minimization. Since the variation problem (1.1) is purely geometric and its solution is independent of parametrization, the solution based on any *parametric method* must be highly nonunique, simply because any surface can be parametrized infinitely many ways. This comment, of course, applies only when we are working at *infinite resolution* (think $\mathcal{F}_{\text{tetra},j}$, $j \to \infty$), when the space of parametric surfaces where we search for our solution allows for all possible parametrizations (of a certain smoothness class) of the solution surface. In theory, the "degree of nonuniqueness" is characterized by the infinite-dimensional group of diffeomorphisms on the solution surface. From a practical point of view one may be more interested in the conformal parametrizations; for a genus 0 surface this reduces the space of solutions from infinite-dimensional to six-dimensional.

When solving (3.1) at a *finite* resolution j, the above consideration suggests the following:

- Problem (3.1) is bound to exhibit many local minimizers with objective values close to the global optimum; see Figure 11. These (nearly optimal) local minimizers correspond to the different parameterizations of the true solution surface.
- For many of these local minimizers, the resulted parametrizations are far from being conformal, as in Figures 12(a) and 13(a), giving rise to triangulations with many triangles of bad aspect ratios. Depending on the problem, the same comment may apply to the global minimizer(s): it may well be the case that at the given resolution, the best possible approximation to the true solution requires the parametrization to be highly nonconformal.
- However, at a fine enough scale j, we expect to see nearly optimal solutions that are nearly conformal.

With the last comment in place, and recalling the fundamental fact from section 3.2 about the relationship of harmonic energy and conformal parametrization, we expect that for most local or global minimizers of Problem (3.1) at a fine enough scale j, we can always trade a small, if not negligible, increase of the Willmore energy for a significant improvement of the "degree of conformality," as measured by harmonic energy, in the parametrization. Therefore, when the quality of parametrization for a numerical solution of (3.1) is a concern, we propose to apply the following postprocessing step based on the minimum Willmore energy W_0 found after solving (3.1): Solve

$$\min_{\mathcal{V}\in\mathbb{R}^{\#V\times 3}} \mathcal{E}(\mathcal{V}) \text{ s.t. } A(\mathcal{V}) = A_0,\ \ V(\mathcal{V}) = V_0,\ \ M(\mathcal{V}) = M_0,\ \ W(\mathcal{V}) \leqslant W_0 + \varepsilon, \tag{3.12}$$

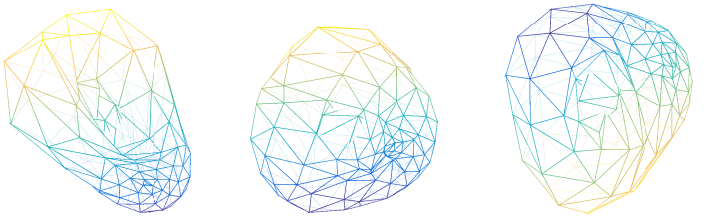

(a) $W = 28.2160$ $\mathcal{E} = 30.9055$ (b) $W = 28.2168$ $\mathcal{E} = 28.5888$ (c) $W = 28.2160$ $\mathcal{E} = 32.0414$

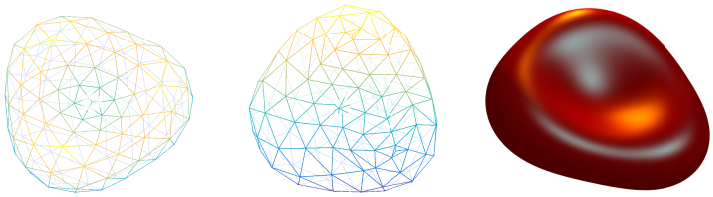

(d) $W = 28.2159$ $\mathcal{E} = 27.1374$ (e) $W = 28.2159$ $\mathcal{E} = 26.6933$ (f)

Figure 11. *Five different local minimizers of* (3.1) *with* $v_0 = 0.5$, $m_0 = 1.05$ *and* $A_0 = 4\pi$, $\mathcal{F} = \mathcal{F}_{\text{tetra},3}$, *obtained from different initial guesses. (For* (c)*, the initial guess is the control mesh of the almost round sphere in Figure* 10(a)*.) The Willmore energies agree in the first* 4 *significant digits; the resulted subdivision surfaces look visually the same* (f)*.*

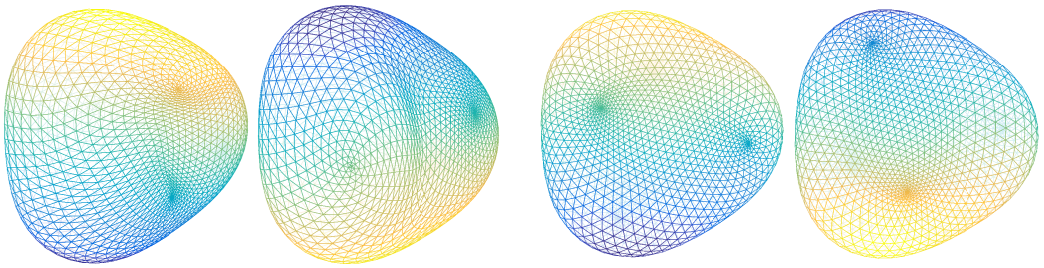

(a) $W = 28.2160$, $\mathcal{E} = 32.0414$ (b) $W = 28.2190$, $\mathcal{E} = 25.3228$

Figure 12. (a) *The control mesh in Figure* 11(c) *subdivided (by the C2g0 scheme)* 2 *more times, displayed with* 2 *different views.* (b) *Solution of* (3.12) *with* $\varepsilon = 0.003$, *using the mesh in Figure* 11(c) *as the initial guess; the solution is again displayed after* 2 *subdivision steps and with the same viewing angles.*

with a small $\varepsilon > 0$. Experiments verify what we expect: an almost negligible increase in Willmore energy allows for a substantial decrease in the harmonic energy. See Figures 12 and 13. Note that these experiments are carried out at pretty low subdivision levels: $j = 3$ (Figure 12) or $j = 4$ (Figure 13); the empirical success is likely attributable to the high accuracy order of the subdivision scheme.

4. Conclusions.

The spherical topology is ubiquitous enough to deserve special attention, at least for the biomembrane problem studied in this work. A specialized high order, high regularity subdivision method is developed. The software implementation in MATLAB and CUDA can be found in http://www.math.drexel.edu/~tyu/C2g0.

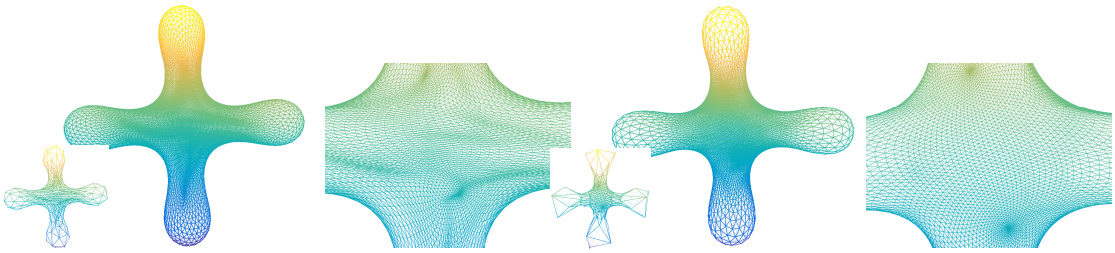

(a) $W = 50.1331$, $\mathcal{E} = 46.2684$ (b) $W = 50.2102$, $\mathcal{E} = 33.5197$

Figure 13. (a) *A C2g0 approximate solution of the Helfrich problem with* $v_0 = 0.4$, $m_0 = 1.8$, $A_0 = 4\pi$, $\mathcal{F} = \mathcal{F}_{\text{tetra},4}$. (b) *Result based on postprocessing the result of* (a) *by* (3.12) *with* $\varepsilon = 0.08$. *For both* (a) *and* (b), *the control mesh (*514 *vertices,* 1024 *faces) is shown at the lower left, the corresponding subdivision surface is displayed based on subdividing the control meshes two more rounds, and the middle of the surface is zoomed in and shown on the right.*

The subdivision method is well-known for its ability to handle arbitrary topology. While this paper goes against this pride, the three-directional box spline underlying the C2g0 scheme can be used to construct a subdivision scheme that handles extraordinary vertices of any valence. It is just that for valence not equal to 3 and 6, Prautzsch and Reif's degree estimate says no flexible C^2 rule is possible, meaning that we can only aim for C^1 rules, as in the Loop scheme.

While the use of harmonic energy for piecewise linear surfaces has been a known idea in applied geometry (for early references, see [7, 12]), the use of harmonic energy for smooth subdivision surfaces seems unexplored previously, especially when applied to the biomembrane problem. The empirical success (section 3.4) stimulates us to ask if a Loop embedding function has a finite harmonic energy with respect to the Bers conformal structure (in the arbitrary topology setting). Note that a Loop subdivision function is only C^1 w.r.t. to the characteristics coordinates defined by the Loop scheme itself; it is not C^1 in Bers's conformal structure. However, $f : \mathcal{M} \to \mathcal{N}$ need not be C^1 but only possess a square-integrable first derivative (i.e., a member of the Sobolev space $H^{1,2}(\mathcal{M}, \mathcal{N})$), in order for the harmonic energy to be defined.

The obvious but difficult question is, what can be said about the numerical solution as an approximation to the true solution of (1.1) as the scale $j \to \infty$?

Acknowledgments. T. Yu would like to acknowledge David Gu, Hartmut Prautzsch, and Aaron Yip for helpful discussions. Tom Duchamp and Rob Kusner both deserve a salute for countless technical communications. He also thanks Michael Overton for initiating and supporting a collaboration between him and the second author.

REFERENCES

[1] L. Bers, *Riemann Surfaces*, Courant Institute of Mathematical Sciences, New York University, New York, 1958.

[2] P. B. Canham, *The minimum energy of bending as a possible explanation of the biconcave shape of the human red blood cell*, J. Theoret. Biol., 26 (1970), pp. 61–76.

[3] A. S. Cavaretta, W. Dahmen, and C. A. Micchelli, *Stationary Subdivision*, Mem. Amer. Math. Soc. 453, AMS, 1991, Providence.

[4] J. Chen, *Numerical Methods and Uniquness for the Canham–Helfrich Model of Biomembranes*, Ph.D. thesis, Department of Mathematics, Drexel University, 2015; also available online from http://www.math.drexel.edu/~tyu/Papers/ChenThesis.pdf.
[5] J. Chen, R. Kusner, T. P.-Y. Yu, and A. Zigerelli, *Numerical Methods for the Canham–Helfrich–Evans Models of Biomembranes*, in preparation, 2015.
[6] C. de Boor, K. Höllig, and S. Riemenschneider, *Box Splines*, Springer-Verlag, Berlin, 1993.
[7] T. Duchamp, A. Certain, A. DeRose, and W. Stuetzle, *Hierarchical Computation of PL Harmonic Embeddings*, preprint, 1997.
[8] E. A. Evans, *Bending resistance and chemically induced moments in membrane bilayers*, Biophys. J., 14 (1974), pp. 923–931, https://dx.doi.org/10.1016/S0006-3495(74)85959-X.
[9] F. Feng and W. S. Klug, *Finite element modeling of lipid bilayer membranes*, J. Comput. Phys., 220 (2006), pp. 394–408, https://dx.doi.org/10.1016/j.jcp.2006.05.023.
[10] W. Freeden, T. Gervens, and M. Schreiner, *Constructive Approximation on the Sphere: With Applications to Geomathematics*, Numer. Math. Sci. Comput., Oxford University Press, New York, 1998.
[11] S. Grundel and T. P.-Y. Yu, *Multiresolution Analysis on a Spherical Domain Based on a Flexible C^2 Subdivision Scheme over a Valence* 3 *Extraordinary Vertex*, preprint, 2011.
[12] X. Gu, Y. Wang, T. Chan, P. Thompson, and S.-T. Yau, *Genus Zero Surface Conformal Mapping and Its Application to Brain Surface Mapping*, in Proceedings of the 18th International Conference on Information Processing in Medical Imaging, C. Taylor and J. Noble, eds., Springer-Verlag, Berlin, 2003, pp. 172–184.
[13] B. Han, T. P.-Y. Yu, and Y. Xue, *Non-interpolatory Hermite subdivision schemes*, Math. Comput., 74 (2005), pp. 1345–1367.
[14] W. Helfich, *Elastic properties of lipid bilayers: Theory and possible experiments*, Z. Nat. C, 28 (1973), pp. 693–703.
[15] J. Jost, *Riemannian Geometry and Geometric Analysis*, 6th ed., Universitext, Springer-Verlag, Berlin, 2011.
[16] K. Karciauskas and J. Peters, *Lens-shaped surfaces and C^2 subdivision*, Computing, 86 (2009), pp. 171–183.
[17] C. T. Loop, *Smooth Subdivision Surfaces Based on Triangles*, Master's thesis, Department of Mathematics, University of Utah, 1987.
[18] D. Nain, S. Haker, A. Bobick, and A. Tannenbaum, *Multiscale 3-D shape representation and segmentation using spherical wavelets*, IEEE Trans. Med. Imaging, 26 (2007), pp. 598–618.
[19] F. J. Narcowich, P. Petrushev, and J. D. Ward, *Localized tight frames on spheres*, SIAM J. Math. Anal., 38 (2006), pp. 574–594, https://doi.org/10.1137/040614359.
[20] J. Peters and U. Reif, *Shape characterization of subdivision surfaces—Basic principles*, Comput. Aided Geom. Design, 21 (2004), pp. 585–599.
[21] J. Peters and U. Reif, *Subdivision Surfaces*, Springer-Verlag, Berlin, 2008.
[22] H. Prautzsch and W. Boehm, *Box splines*, in Handbook of Computer Aided Geometric Design, North-Holland, Amsterdam, 2002, pp. 255–282, https://doi.org/10.1016/B978-044451104-1/50011-3.
[23] H. Prautzsch and U. Reif, *Degree estimates for C^k-piecewise polynomial subdivision surfaces*, Adv. Comput. Math., 10 (1999), pp. 209–217.
[24] U. Reif, *A unified approach to subdivision algorithms near extraordinary points*, Comput. Aided Geom. Design, 12 (1995), pp. 153–174.
[25] U. Reif, *A degree estimate for subdivision surfaces of higher regularity*, Proc. Amer. Math. Soc., 124 (1996), pp. 153–174.
[26] P. Schröder and W. Sweldens, *Spherical wavelets: Efficiently representing functions on the sphere*, in Proceedings of the Conference on Computer Graphics (SIGGRAPH 95), 1995, pp. 161–172.
[27] U. Seifert, *Configurations of fluid membranes and vesicles*, Adv. Phys., 46 (1997), pp. 13–137.
[28] J. Stam, *Exact evaluation of Catmull–Clark subdivision surfaces at arbitrary parameter values*, in Proceedings of the 25th Annual Conference on Computer Graphics and Interactive Techniques (SIGGRAPH 98), New York, ACM, 1998, pp. 395–404, https://doi.org/10.1145/280814.280945.
[29] J. Warren and H. Weimer, *Subdivision Methods for Geometric Design: A Constructive Approach*, Morgan Kaufmann, Burlington, MA, 2001.

[30] Y. Xue, T. P.-Y. Yu, and T. Duchamp, *Jet subdivision schemes on the k-regular complex*, Comput. Aided Geom. Design, 23 (2006), pp. 361–396.
[31] D. Zorin, *A method for analysis of C^1-continuity of subdivision surfaces*, SIAM J. Numer. Anal., 37 (2000), pp. 1677–1708.
[32] D. Zorin, *Smoothness of subdivision on irregular meshes*, Constr. Approx., 16 (2000), pp. 359–397.